

# Boundary effects in two-band superconductors

Andrea Benfenati,<sup>1,\*</sup> Albert Samoilenko,<sup>1</sup> and Egor Babaev<sup>1</sup>

<sup>1</sup>*Department of Physics, The Royal Institute of Technology, Stockholm SE-10691, Sweden*

(Dated: January 21, 2022)

We present a microscopic study of the behavior of the order parameters near boundaries of a two-band superconducting material, described by the standard tight-binding Bardeen-Cooper-Schrieffer model. We find superconducting surface states. The relative difference between bulk and surface critical temperatures is a nontrivial function of the interband coupling strength. For superconductors with weak interband coupling, boundaries induce variations of the gaps with the presence of multiple length scales, despite non-zero interband Josephson coupling.

## INTRODUCTION

The majority of the superconductors of current interest have multiple superconducting bands [1, 2] with a widely varying strength of the interband coupling. Understanding the boundary effects of a superconductor is important since, superconducting currents are concentrated near the surfaces, and the physics of boundaries controls vortex entry barriers and thus the onset of dissipation. Moreover, the behavior of the gaps near boundaries is crucial in small superconducting devices, such as superconducting nanowires and single-photon detectors, where multiband materials are utilized [3].

In the last decades, topological superconductors have attracted particular interest. These materials exhibit topological surface currents, the observation of which is searched as a smoking gun for topological superconductivity and can potentially be used to understand the nature of it. Among the candidate materials, there are compounds with complicated multiband structure, raising the need of an understanding of the surface's properties [4]. For conventional and exotic multiband materials, the gaps are characterized by variety of probes, some of which selectively probe surfaces, while others are dominated by the bulk response [5–12]. The gap ratio is a characteristic quantity that allows one to get an insight into physics of Cooper pairing. In the presence of surface superconductivity, it therefore important to study the gap ratio properties both in the bulk and near the boundaries.

The series of experimental works [13–15] reported that, on the surface of ZrB<sub>12</sub>, the characteristics of the superconducting gaps are widely different compared to the bulk. Refs. [16, 17] suggested that ZrB<sub>12</sub> is a multiband superconductor with weak interband coupling. A partial summary of the experimentally observed discrepancies, concerning surface/bulk gap structure, can be found in Table I in [14]. The surface effects are quite strong compared to other reported experimental examples of enhanced surface superconductivity [18–24]. To explain this, it was proposed to search for a mechanism of different phonon-electron interaction on the surface of the material [25]. However, the recent works [26, 27] reported

that enhanced superconductivity near the boundary is a generic property of the standard single-band Bardeen-Cooper-Schrieffer model. Namely, it was found that the presence of Friedel oscillations near the boundary induces an increase in the density of states, at a microscopic length scale, yielding a higher critical temperature [27]. The solution has multiple length scales and depends on the coherence length.

That raises the question of the nature of surface states in a generic multi-band Bardeen-Cooper-Schrieffer model [1, 2], where multiple length- and energy-scales are present. In this work, we analyze the behaviour of the two superconducting gaps as a function of the interband coupling. We focus on the limit of a clean ideal surface, with negligible single-particle interband scattering. [28]

## THE MODEL

We consider a Fermi-Hubbard Hamiltonian describing a two-band *s*-wave superconductor. For a *d* dimensional hypercubic lattice it reads

$$H = \sum_{i,j,\sigma,\alpha} \psi_{i\sigma\alpha}^\dagger h_{ij\sigma\alpha} \psi_{j\sigma\alpha} - \sum_{i\alpha,\beta} V_{\alpha\beta} \psi_{i\uparrow\alpha}^\dagger \psi_{i\downarrow\alpha}^\dagger \psi_{i\downarrow\beta} \psi_{i\uparrow\beta}. \quad (1)$$

The roman indices *i, j* label the position on a lattice with *N* lattice points.  $\sigma = \uparrow, \downarrow$  indicates the spin, while  $\alpha, \beta = 1, 2$  label the component. Then  $h_{ij\sigma\alpha} = -\mu\delta_{ij} - t\delta_{|i-j|,1}$ , where  $|i-j| = 1$  if *i* and *j* are neighboring points in hypercubic lattice.  $\mu$  is the chemical potential and *t* the hopping coefficient. In order to ensure the Hamiltonian to be hermitian, we have  $h_{ij\sigma\alpha} = h_{ji\sigma\alpha}^*$  and  $V_{\alpha\beta} = V_{\beta\alpha}^*$ . Then, following the steps in [29], we perform the mean field approximation. Introducing the Nambu spinors

$$\begin{aligned} \Psi_\alpha^\dagger &= (\psi_{1\uparrow\alpha}^\dagger, \dots, \psi_{N\uparrow\alpha}^\dagger, \psi_{1\downarrow\alpha}, \dots, \psi_{N\downarrow\alpha}) \\ \Psi_\alpha &= (\psi_{1\uparrow\alpha}, \dots, \psi_{N\uparrow\alpha}, \psi_{1\downarrow\alpha}^\dagger, \dots, \psi_{N\downarrow\alpha}^\dagger)^T, \end{aligned} \quad (2)$$

the total mean field Hamiltonian reads

$$H_{MF} = \sum_{\alpha=1}^2 \Psi_{\alpha}^{\dagger} H_{\alpha} \Psi_{\alpha}. \quad (3)$$

$H_{\alpha}$  is the  $\alpha$ -band Hamiltonian, defined as

$$H_{\alpha} = \begin{pmatrix} h_{\uparrow\alpha} & \Delta_{\alpha} \\ \Delta_{\alpha}^{\dagger} & -h_{\downarrow\alpha}^T \end{pmatrix}, \quad (4)$$

where the elements  $h_{ij\sigma\alpha}$  have been defined above. Finally, the self-consistency equations for the gaps are:

$$\Delta_{i\alpha} = \sum_{\beta=1}^2 V_{\alpha\beta} \langle c_{i\uparrow\beta} c_{i\downarrow\beta} \rangle_{\beta}. \quad (5)$$

The thermal average  $\langle \cdot \rangle_{\beta}$  means it is performed over the eigenvalues of the hamiltonian  $H_{\beta}$ . We can rewrite the self consistency equation by introducing the auxiliary vectors  $(\mathbf{e}_i)_j = \delta_{i,j}$  and  $(\mathbf{h}_i)_j = \delta_{j,i+N}$  as

$$\Delta_{i\alpha} = - \sum_{\beta=1}^2 V_{\alpha\beta} \mathbf{e}_i f(H_{\beta}) \mathbf{h}_i, \quad (6)$$

with  $f(x) = (1 + e^{x/T})^{-1}$  being the Fermi-Dirac function. We solve self-consistently for the gaps  $\Delta_{i\alpha}$ , using Chebyshev polynomial expansion method [30–32], with polynomial up to order 1000. The convergence criterion we adopt is  $|\Delta_{i\alpha}^{(n+1)} - \Delta_{i\alpha}^{(n)}|/|\Delta_{i\alpha}^{(n)}| \leq 10^{-8}$ , where  $n$  numbers the iteration. We consider both a 1D lattice with  $N = 1000$  sites and a 2D square lattice with  $N_x N_y = 60 \times 60$ . The solver is a custom CUDA implementation. To calculate the critical temperatures, we solve the linearized version of the self consistency equation (6). For details, see [26].

## RESULTS

### Effects of interband coupling

We begin by analyzing a 2-band system with weak interband coupling and similar intraband interaction in two bands. The model is rescaled so that all the quantities are given in units of the hopping coefficient  $t$ . We fix  $\mu = 0$ , i.e. half filled bands,  $V_{11} = 1.35$  and  $V_{22} = 1.36$ . We compare the results for non-zero interband interaction  $V_{12}$  with the case where the bands are decoupled, i.e.  $V_{12} = 0.0$ . In the latter, the problem is reduced to two copies of the model studied in [26] and shown to have two different critical temperatures, one for bulk states and one for boundary states. We denote by  $T_{c1}$  the bulk critical temperature, i.e. when the order parameter vanishes in the bulk.  $T_{c2}$  is the boundary critical temperature, i.e. when the order parameter vanishes on the boundaries of the superconductor. When  $V_{12} = 0$  the

critical temperatures in the system are:  $T_{c1}^{\text{band1}} = 0.0429$  and  $T_{c2}^{\text{band1}} = 0.0536$  for band 1,  $T_{c1}^{\text{band2}} = 0.045$  and  $T_{c2}^{\text{band2}} = 0.0562$  for band 2. Hence, in this example, the second band has a critical temperatures 5% higher than the first. Figure 1 shows the numerically obtained gaps  $\Delta_1$  and  $\Delta_2$ , displayed at various temperatures and interband coupling. In accordance with the results obtained by different analytical and numerical methods in [26], when  $V_{12} = 0$ , the boundary-enhancement of each gap decays to the bulk value with independent coherence length. As the coupling is turned on,  $U(1)$  is broken,

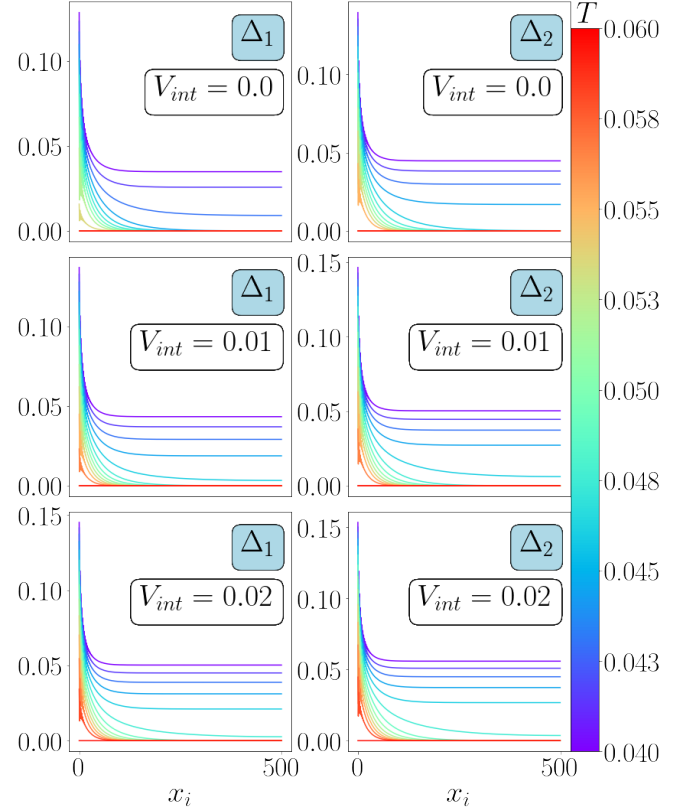


FIG. 1. Numerical solution for the two gaps at different values of the interband coupling. The boundary is located at  $x = 0$ . For  $V_{int} = 0.0$ , the two bands have different boundary and bulk critical temperatures. When the interband interaction is on, the two bands present the same critical temperatures. Yet, the weak interband coupling does not drastically affect the structure of the solution. The gaps exhibit different enhancement near the boundary and the overall solution shows the presence of different length scales. For  $V_{12} = 0.01$  we have  $T_{c1} = 0.0458$  and  $T_{c2} = 0.0573$ . For  $V_{12} = 0.02$  the critical temperatures increase respectively to  $T_{c1} = 0.0472$ ,  $T_{c2} = 0.0591$ . Here we show only the left half of the system.

since the carriers in the individual bands are no longer independently conserved and there are no independent transitions for different bands.

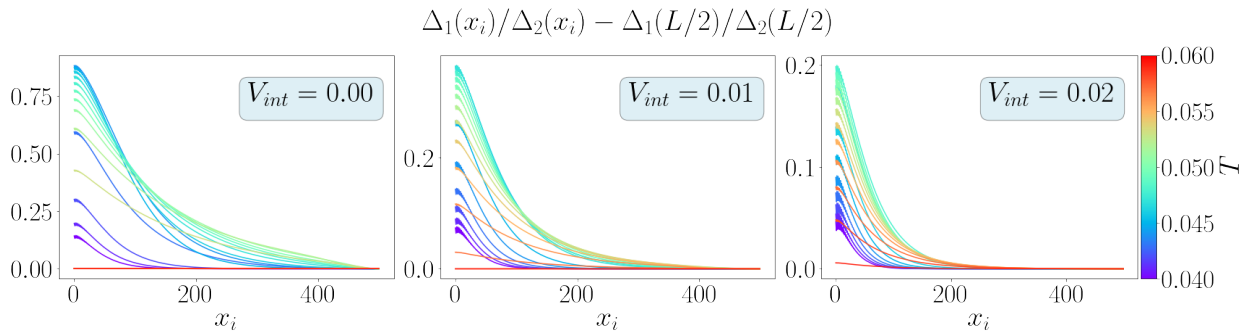


FIG. 3. Plot of gap ratios shifted by the bulk value. We can notice that the gaps ratio near the surface is enhanced compared to the bulk value. The presence of weak inter-band coupling does not qualitatively change this effect. Moreover, the length scale of the penetration into the bulk shows a non monotonic behaviour as a function of  $T$ , as more accurately displayed in Figure 4. We show only half of the system (500 out of  $L = 1000$  sites), since the second half is entirely symmetrical. The parameters used for this simulations are  $V_{11} = 1.35$ ,  $V_{22} = 1.36$  and  $\mu = 0$ .

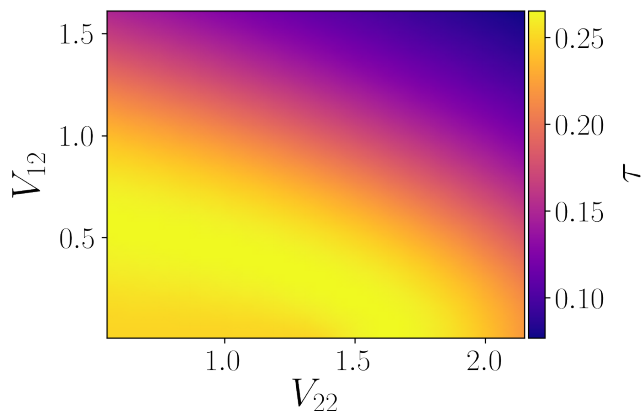


FIG. 2. Relative increase of the boundary critical temperature with respect to the bulk critical temperature as a function of the pairing potential of the second band  $V_{22}$  and of the inter-band coupling  $V_{12}$ . We define  $\tau = (T_{c2} - T_{c1})/T_{c1}$ . For a given value of  $V_{22}$ ,  $\tau$  exhibit a non monotonic behavior as a function of interband coupling  $V_{12}$ .  $V_{11} = 1.35$  and  $\mu = 0$ .

#### The relative behavior of the gaps in two-band systems: boundaries vs bulk

A useful characteristic of a multiband superconductor is the ratio of the gaps of different bands, whose temperature dependence can give insights into nature of pairing in the material. Figure 3 shows the gaps ratio shifted by its bulk values at various temperatures  $T$  and inter-band coupling  $V_{12}$  for a 1D system as a function of distance from the boundary. The system we consider first has the intraband potential of the second band only 1% bigger than the first one, namely  $V_{11} = 1.35$  and  $V_{22} = 1.36$ .

Even for these similar gap characteristics, we find that the gaps ratio can be different on the boundary of a superconductor compared to its bulk value, when the inter-band coupling is weak. Figure 3 displays the results for  $V_{12} = 0.01$ ,  $0.02$  and compares them to the decoupled-bands case.

Then, for non-zero  $V_{12}$ , the bulk critical temperatures become the same for both bands. Also the surface critical temperature is only one. The gaps behaviour near the boundaries is nontrivial as it includes relative variations of the gap values. In the case displayed in Figure 1 we have  $T_{c1} = 0.0458$  and  $T_{c2} = 0.0573$  for  $V_{12} = 0.01$ ;  $T_{c1} = 0.0472$  and  $T_{c2} = 0.0591$  for  $V_{12} = 0.02$ .

We conclude this section by moving beyond the weak interband coupling regime and investigate the relative increase of the boundary critical temperature  $T_{c2}$ , with respect to the bulk temperature  $T_{c1}$ , as a function of inter-band coupling  $V_{12}$ . To efficiently measure this increase, we define  $\tau = (T_{c2} - T_{c1})/T_{c1}$ . The numerical solutions for a one dimensional model are shown on the Figure 2 for various values of  $V_{22}$ . We find that the dependence is non-trivial: at relatively weak interband coupling,  $\tau$  first increases with  $V_{12}$  and then, it starts to decrease.

In particular, we notice that the both the gaps and their ratio are enhanced near the ends of the sample, and this enhancement decays into the interior of the superconductor on a macroscopic length scale. The surface gaps ratio deviation has not only a strong temperature dependence in magnitude, but also its length scale varies as a function of  $T$ . We can study the latter's behavior in further details by fitting the tails (i.e. after  $N=50$  sites from the boundary) of the gaps ratio deviations reported in Figure 3, with an exponential function  $f(x) \propto e^{-x/\xi}$ . Here,  $\xi(T)$  measures the length scale of the decay into the bulk. The result, reported in Figure 4 confirms the non-monotonic behavior of  $\xi(T)$  as a function of  $T$ .

Discussion concerning the existence of multiple length scales in multiband material, previously only focused on vortex physics [33–35]. The behavior of the surface states that we find is a new example of existence of multiple length scales in multiband materials, despite non-zero

Josephson coupling. The long range character associated with the relative variations of the gaps, and its non-monotonicity is consistent with the conclusions obtained for the vortex core solutions in weakly interacting two-band systems in [33, 34]. At higher values of the interband coupling, we can notice that the relative variation of the gaps profile near the surfaces decreases, both in amplitude and in its spatial extension, as Figure 5 reports. This remains consistent with the hybridization of bulk coherence lengths and their dependence on interband coupling strength [33]. When the interband coupling  $V_{12}$  becomes of the same order of magnitude as the intraband coupling  $V_{11}$  and  $V_{22}$ , e.g.  $V_{12} = 1.0$ , the enhancement of the gaps ratio basically disappears. Note that the disappearance of this variation is similar to the condition for the disappearance of the second coherence lengths in the clean two-band BCS semi-classical model found in [33]. This confirms that the width of the boundary states, in two band states, is in general determined by two bulk coherence lengths.

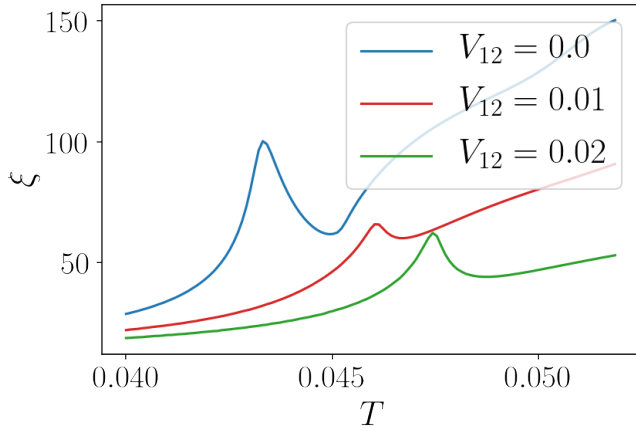


FIG. 4. Long range asymptotic decay length scale  $\xi(T)$  of the gaps ratio deviation displayed in Figure 3.  $\xi(T)$  is plotted as a function of the temperature  $T$  and for different values of the interband coupling. The non monotonic behavior as a function of  $T$  is clearly visible. We obtain  $\xi(T)$  by fitting the tails (i.e. after  $N = 50$  sites from the boundary) of the gaps ratio deviation using an exponential function  $f(x) \propto e^{-x/\xi}$ , for the different values of  $T$  and  $V_{12}$ . The remaining parameters used in the simulations are  $V_{11} = 1.35$ ,  $V_{22} = 1.36$  and  $\mu = 0$ .

Next we consider the boundary states when the difference between the intraband potential is greater. Specifically we consider  $V_{11} = 1.35$  and  $V_{22} = 1.68$ . The upper panel of Figure 6 shows the gaps  $\Delta_1$  (solid line) and  $\Delta_2$  (dashed line) at various temperatures. The bottom panel displays the variation of the gaps ratio with respect to the bulk value. Here the interband potential is set to be  $V_{12} = 0.1$ . We can see a moderate increase of  $V_{22}$  yields a substantial variation of the relative gap values near the surface compared to Figure 5.

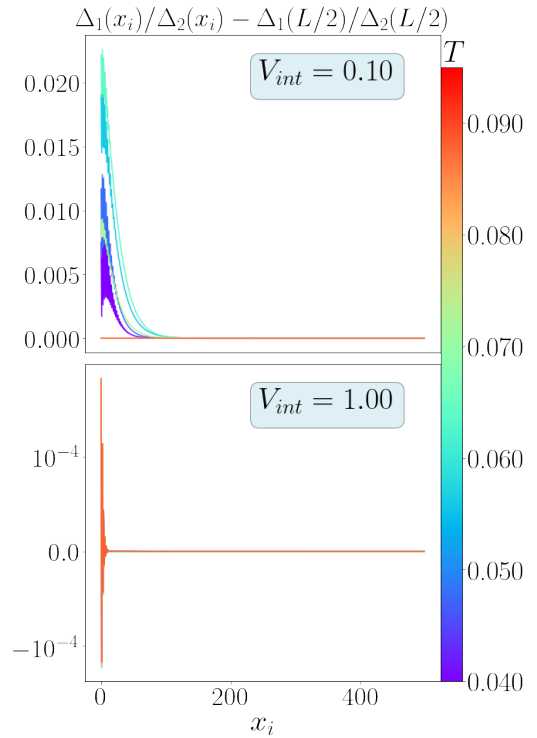


FIG. 5. Suppression of the relative gap variations at stronger interband coupling. We can notice that the gaps ratio change near the boundary is an order of magnitude smaller for  $V_{12} = 0.1$  than for  $V_{12} = 0.01$ . For strong interband coupling  $V_{12} = 1$ , in the simplest two-band model, the surface-induced change of the gaps ratio is negligible. Also in this case we show only half of the system (500 out of  $N = 1000$  sites), since the second half is symmetrical. The parameters used for these calculations are  $V_{11} = 1.35$ ,  $V_{22} = 1.36$  and  $\mu = 0$ .

### Surface effects in two-dimensions and corner states

In 2D and 3D single-component BCS models there are superconducting corner and edge states with relative critical temperature higher than the bulk critical temperature [26, 29]. In this section, we consider the gaps ratio spatial profile in a two dimensional two-band system. In 2D we have edges and corners, therefore we can associate  $T_{c2}$  as the mean-field critical temperature for edge superconductivity, and  $T_{c3}$  as the mean-field critical temperature for corner superconductivity. In a single-band BCS 2D system,  $T_{c3} > T_{c2}$ , as shown in [29]. We study the two-band system for  $T < T_{c1}$ ,  $T_{c1} < T < T_{c2}$  and  $T_{c2} < T < T_{c3}$ . Studying the boundary effects in two dimensions is challenging, as it requires numerically solving significantly large systems, to avoid the finite-size effects' influence on the resulting states. Figure 7 shows the gaps ratio shifted by its value in the bulk, and the two gaps  $\Delta_1$ ,  $\Delta_2$ . We can notice that the boundary states exist at much smaller length scales than the size of the sample. Both for the bulk ( $T = 0.75$ ) and the edge ( $T = 0.77$ ) states the gaps ratio is enhanced along the system bound-

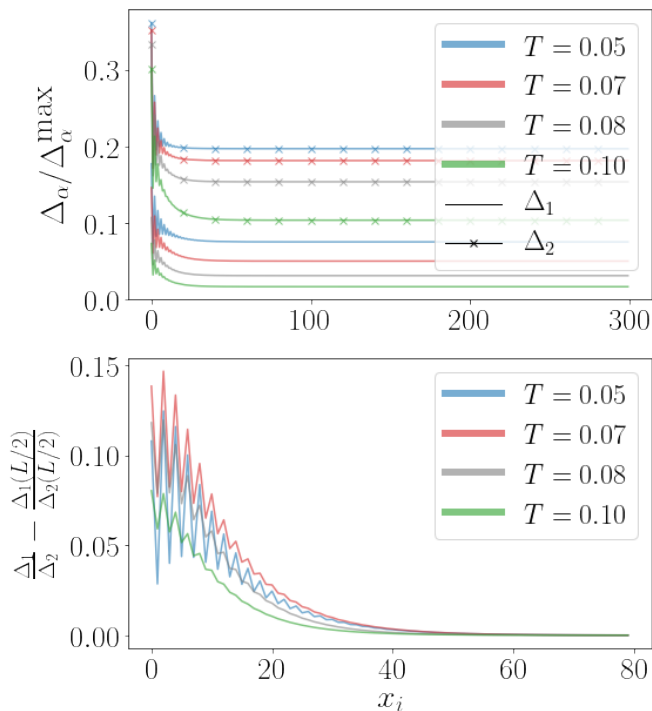


FIG. 6. Numerically obtained order parameters for different values of the  $T$ . In this case, we study a coupled two-band system where the difference between the two intraband potentials  $V_{11}$  and  $V_{22}$  is higher, namely 25%. The upper panel displays the gaps  $\Delta_1$  (solid line) and  $\Delta_2$  (crossed line) independently. The bottom panel reports the gaps ratio near-surface spatial variation relative to the bulk value. For both panels we fixed  $V_{12} = 0.1$ . We can notice that the modest increase in  $V_{22}$  results in substantially larger variation of the gap ratio near the boundary. Both results were obtained for a system with  $N = 1000$  and  $\mu = 0$ .

aries. When the temperature exceeds the edge critical temperature  $T_{c2} = 0.774$ , the superconductivity ceases to exist along the boundaries, but remains in the four corners. We observe that in the corners there is the largest variation of the gaps ratio, which decays into the bulk at a macroscopic length scale.

## CONCLUSIONS

Since most of superconductors of current interest are multiband, and there are experimental puzzles, such as the surface gap enhancement in  $\text{ZrB}_{12}$  [13–15] it is important to understand the boundary effects in multiband superconducting materials.

We studied the boundary effects in the standard two-band Bardeen-Cooper-Schrieffer theory of superconductivity. We showed that, at the level of mean-field theory, the system has multiple critical temperatures, associated to the presence of boundary states.

We found that the dependence of the critical tem-

peratures on the value of interband coupling is non-monotonic.

Moreover, when interband coupling is relatively weak, the behavior of the gaps near the boundaries presents multiple coherence lengths and a relative variation of the gaps values.

In dimensions higher than one, the effects are stronger in the sample's corners. The relative variation of the gaps values extends into the superconductor with a large temperature-dependent length scale. This should be of particular importance for critical currents in small superconducting devices. The enhanced surface superconductivity may be harvested to improve superconducting-nanowire-based single photon detectors. A material with increased gap near the surface is expected to enhance vortex entry barrier which can yield less dark counts. An interesting question for further studies is the effect of boundary-induced single particle scattering [36] on the states we report.

## ACKNOWLEDGEMENTS

The work was supported by the Swedish Research Council Grants No. 642-2013-7837, 2016-06122, 2018-03659, the Göran Gustafsson Foundation for Research in Natural Sciences and Medicine, Olle Engkvists Stiftelse.

---

\* alben@kth.se

- [1] H. Suhl, B. T. Matthias, and L. R. Walker, Bardeen-cooper-schrieffer theory of superconductivity in the case of overlapping bands, *Phys. Rev. Lett.* **3**, 552 (1959).
- [2] V. Moskalenko, Superconductivity in metals with overlapping energy bands, *Fiz. Metal. Metalloved* **8**, 2518 (1959).
- [3] H. Shibata, T. Akazaki, and Y. Tokura, Fabrication of mgb2 nanowire single-photon detector with meander structure, *Applied Physics Express* **6**, 023101 (2013).
- [4] A. Bouhon and M. Sigrist, Current inversion at the edges of a chiral p-wave superconductor, *Physical Review B* **90**, 220511 (2014).
- [5] A. Kreisel, P. J. Hirschfeld, and B. M. Andersen, On the remarkable superconductivity of fese and its close cousins, *Symmetry* **12**, 1402 (2020).
- [6] A. Chubukov, Pairing mechanism in fe-based superconductors, *Annu. Rev. Condens. Matter Phys.* **3**, 57 (2012).
- [7] I. Mazin and V. Antropov, Electronic structure, electron-phonon coupling, and multiband effects in mgb2, *Physica C: Superconductivity* **385**, 49 (2003).
- [8] A. P. Mackenzie, T. Scaffidi, C. W. Hicks, and Y. Maeno, Even odder after twenty-three years: the superconducting order parameter puzzle of sr 2 ruo 4, *npj Quantum Materials* **2**, 1 (2017).
- [9] R. Sharma, S. D. Edkins, Z. Wang, A. Kostin, C. Sow, Y. Maeno, A. P. Mackenzie, J. S. Davis, and V. Madhavan, Momentum-resolved superconducting energy gaps



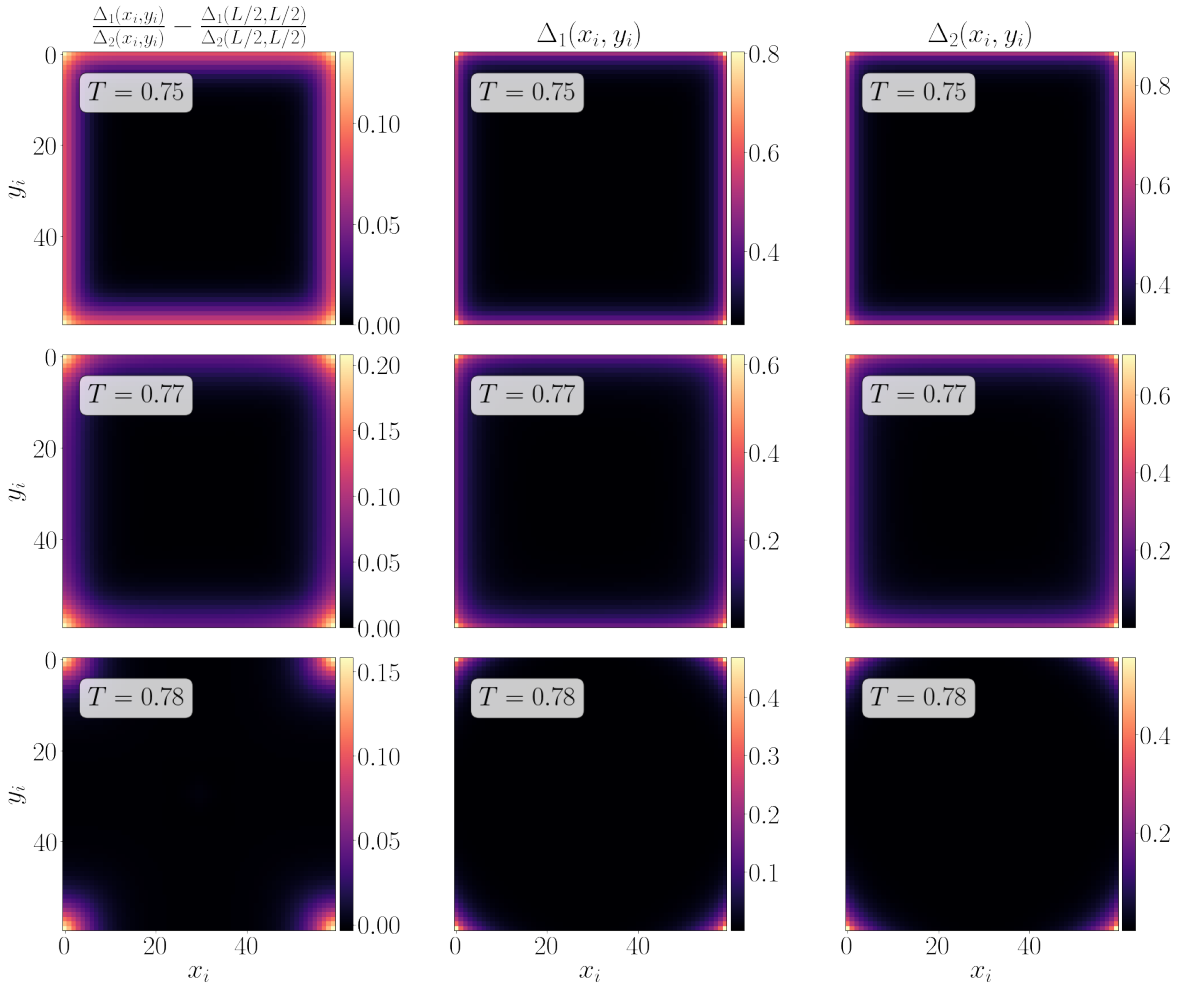


FIG. 7. Plot of the gaps ratio shifted by the bulk value (left column),  $\Delta_1$  (center column) and  $\Delta_2$  (right column) in two dimensions for increasing temperatures. The bulk critical temperature for the system reads  $T_{c1} = 0.759$  and the edge critical temperature is  $T_{c2} = 0.774$ . Therefore the first row shows the bulk superconductivity, the second row shows the edge superconductivity and the third row shows the state where the gap survives only in the corners. Below the corner critical temperature, i.e. for bulk and edge states we can notice the gradient of the gaps ration localized along the system's boundaries. The increase is more pronounced above the bulk critical temperature, i.e. with edge states. When  $T_{c2} < T < T_{c3}$  superconductivity survives in the four corners, where also the gaps ratio undergoes significant enhancement, penetrating into the bulk with macroscopic length scale.

- of sr2ruo4 from quasiparticle interference imaging, Proceedings of the National Academy of Sciences **117**, 5222 (2020).
- [10] J. Böker, P. A. Volkov, K. B. Efetov, and I. Eremin, s+ i s superconductivity with incipient bands: Doping dependence and stm signatures, Physical Review B **96**, 014517 (2017).
- [11] S. Zhao, H.-Y. Song, L. Hu, T. Xie, C. Liu, H. Luo, C.-Y. Jiang, X. Zhang, X. Nie, J.-Q. Meng, *et al.*, Observation of soft leggett mode in superconducting cakfe 4 as 4, Physical Review B **102**, 144519 (2020).
- [12] G. Rubio-Bollinger, H. Suderow, and S. Vieira, Tunneling spectroscopy in small grains of superconducting mgb<sub>2</sub>, Phys. Rev. Lett. **86**, 5582 (2001).
- [13] M. Tsindlekht, G. Leviev, I. Asulin, A. Sharoni, O. Millo, I. Felner, Y. B. Paderno, V. Filippov, and M. Belogolovskii, Tunneling and magnetic characteristics of superconducting zrb 12 single crystals, Physical Review B **69**, 212508 (2004).
- [14] M. Belogolovskii, I. Felner, and V. Shaternik, Zirconium dodecaboride, a novel superconducting material with enhanced surface characteristics, in *Boron Rich Solids* (Springer, 2010) pp. 195–206.
- [15] R. Khasanov, D. Di Castro, M. Belogolovskii, Y. Paderno, V. Filippov, R. Brütsch, and H. Keller, Anomalous electron-phonon coupling probed on the surface of superconductor zr b 12, Physical Review B **72**, 224509 (2005).
- [16] V. Gasparov, N. Sidorov, and I. Zver'Kova, Two-gap superconductivity in zr b 12: temperature dependence of critical magnetic fields in single crystals, Physical Review B **73**, 094510 (2006).
- [17] P. Biswas, F. Rybakov, R. Singh, S. Mukherjee, N. Parzyk, G. Balakrishnan, M. Lees, C. Dewhurst,

- E. Babaev, A. Hillier, *et al.*, Coexistence of type-i and type-ii superconductivity signatures in  $\text{ZrB}_{12}$  probed by muon spin rotation measurements, *Physical Review B* **102**, 144523 (2020).
- [18] H. Fink and W. Joiner, Surface nucleation and boundary conditions in superconductors, *Physical Review Letters* **23**, 120 (1969).
- [19] R. Lortz, T. Tomita, Y. Wang, A. Junod, J. Schilling, T. Masui, and S. Tajima, On the origin of the double superconducting transition in overdoped  $\text{YBa}_2\text{Cu}_3\text{O}_x$ , *Physica C: Superconductivity* **434**, 194 (2006).
- [20] E. Janod, A. Junod, T. Graf, K.-Q. Wang, G. Triscone, and J. Muller, Split superconducting transitions in the specific heat and magnetic susceptibility of  $\text{YBa}_2\text{Cu}_3\text{O}_x$  versus oxygen content, *Physica C: Superconductivity* **216**, 129 (1993).
- [21] R. A. Butera, High-resolution heat capacity of  $\text{YBa}_2\text{Cu}_3\text{O}_{6.9}$  over the superconducting transition region, *Physical Review B* **37**, 5909 (1988).
- [22] I. Khlyustikov, Critical magnetic field of surface superconductivity in lead, *Journal of Experimental and Theoretical Physics* **113**, 1032 (2011).
- [23] I. Khlyustikov, Surface superconductivity in lead, *Journal of Experimental and Theoretical Physics* **122**, 328 (2016).
- [24] I. Mangel, I. Kapon, N. Blau, K. Golubkov, N. Gavish, and A. Keren, Stiffnessometer: A magnetic-field-free superconducting stiffness meter and its application, *Physical Review B* **102**, 024502 (2020).
- [25] V. Ginzburg, On surface superconductivity, *Phys. Letters* **13** (1964).
- [26] A. Samoilenka and E. Babaev, Boundary states with elevated critical temperatures in bardeen-cooper-schrieffer superconductors, *Physical Review B* **101**, 134512 (2020).
- [27] A. Samoilenka and E. Babaev, Microscopic derivation of superconductor-insulator boundary conditions for ginzburg-landau theory revisited. enhanced superconductivity with and without magnetic field (2020), arXiv:2011.09519 [cond-mat.supr-con].
- [28] The effects of single-particle interband scattering were already studied in [36]. The effects of atomic-scale surface imperfections were addressed in [26] for a single-band material.
- [29] A. Samoilenka, M. Barkman, A. Benfenati, and E. Babaev, Pair-density-wave superconductivity of faces, edges, and vertices in systems with imbalanced fermions, *Physical Review B* **101**, 054506 (2020).
- [30] A. Weiße, G. Wellein, A. Alvermann, and H. Fehske, The kernel polynomial method, *Rev. Mod. Phys.* **78**, 275 (2006).
- [31] L. Covaci, F. M. Peeters, and M. Berciu, Efficient numerical approach to inhomogeneous superconductivity: The chebyshev-bogoliubov-de gennes method, *Phys. Rev. Lett.* **105**, 167006 (2010).
- [32] Y. Nagai, Y. Ota, and M. Machida, Efficient numerical self-consistent mean-field approach for fermionic many-body systems by polynomial expansion on spectral density, *Journal of the Physical Society of Japan* **81**, 024710 (2012), <https://doi.org/10.1143/JPSJ.81.024710>.
- [33] M. Silaev and E. Babaev, Microscopic theory of type-1.5 superconductivity in multiband systems, *Phys. Rev. B* **84**, 094515 (2011).
- [34] M. Silaev and E. Babaev, Microscopic derivation of two-component ginzburg-landau model and conditions of its applicability in two-band systems, *Physical Review B* **85**, 134514 (2012).
- [35] J. Carlström, E. Babaev, and M. Speight, Type-1.5 superconductivity in multiband systems: Effects of interband couplings, *Phys. Rev. B* **83**, 174509 (2011).
- [36] E. Bascones and F. Guinea, Surface effects in two-band superconductors: Application to  $\text{MgB}_2$ , *Physical Review B* **64**, 214508 (2001).